Geomechanics and Engineering, *Vol. 24, No. 5 (2021) 457-470*
DOI: https://doi.org/10.12989/gae.2021.24.5.457

Evaluation of failure mode of tunnel-type anchorage for a suspension bridge via scaled model tests and image processing

Seunghwan Seo[a], Hyungsung Lim[b] and Moonkyung Chung*

Department of Underground Space Safety Research Center, Korea Institute of Civil Engineering and Building Technology (KICT), Goyang-si, Gyeonggi-do 10223, Republic of Korea

(Received March 24, 2020, Revised November 11, 2020, Accepted February 18, 2021)

Abstract. In this study, the pull-out behavior of a tunnel-type anchorage for suspension bridges was investigated using experimental tests and image processing analyses. The study focused on evaluating the initial failure behavior and failure mode of the tunnel-type anchorage. In order to evaluate the failure mode of tunnel-type anchorage, a series of scaled model tests were conducted based on the prototype anchorage of the Ulsan Grand Bridge. In the model tests, the anchorage body and surrounding rocks were fabricated using a gypsum mixture. The pull-out behavior was investigated under plane strain conditions. The results of the model tests demonstrate that the tunnel-type anchorage underwent a wedge-shaped failure. In addition, the failure mode changed according to the differences in the physical properties of the surrounding rock and the anchorage body and the size of the anchor plate. The size of the anchor plate was found to be an important parameter that determines the failure mode. However, the difference in physical properties between the surrounding rock and the anchorage body did not affect its size. In addition, this study analyzed the initial failure behavior of the tunnel-type anchorage through image analysis and confirmed that the failure was sequentially transferred from the inside of the tunnel to the surrounding rock according to the image analysis. The reasonable failure mode for the design of the tunnel-type anchorage should be wedge-type rather than pull-out type.

Keywords: tunnel-type anchorage; pull-out behavior; failure mode; image processing; scaled model test

1. Introduction

The anchorages of a suspension bridge are subjected to pull-out loads induced by the tension of the main cables. Suspension bridges can be classified into two types according to anchorage design: self-anchored and ground-anchored (ASCE 1979, Hong *et al*. 2014). Ground-anchored suspension bridges are divided into gravity-type, tunnel-type, and cavern-type. Gravity-type anchorages can be applied regardless of the ground conditions to resist the cable load due to the weight of the anchor. In addition, the support mechanism of gravity-type anchorages is reliable. However, the anchorage structure tends to be heavy. Therefore, a high volume of concrete and a large construction space are required for such anchorages. The tunnel-type anchorage involves excavating a tunnel in the ground and filling it with steel and concrete to support the cable load of the bridge (ASCE 1979, Hong *et al*. 2014, Dakeuchi and Yoshida 1984). Therefore, tunnel-type anchorages exhibit a high performance–cost ratio and rarely disturb the surrounding environment. The tunnel-type anchorage, therefore, may be preferable from the viewpoint of space and environmental concerns. In addition, the Design Specifications for Highway Suspension Bridges (China Communication Press 2015) recommends that tunnel anchorage construction be considered when site conditions are favorable. As the suspended span length of cable supported bridges increases, the main cable tension and supporting load of the anchorage increase (Fig. 1). Therefore, the anchorage volume also increases. Tunnel-type anchorage should be applied using solid ground if ground conditions such as hard rock or soft rock are satisfied. The tunnel-type anchorage can secure a load that is 20-25% that of the gravity-type anchorage under solid ground conditions (Han *et al*. 2019, Zhang *et al*. 2015)

Tunnel-type anchorages, however, are more sensitive to ground conditions, unlike gravity-type anchorages. In particular, the failure mode depends on aspects such as the characteristics of the surrounding rock and the anchorage cross-sectional shape. Therefore, the pull-out resistance and activity stability are considered when designing such anchorages. During the design process, the failure mode is analyzed, and the pull-out resistance and stability of operation are examined according to the characteristics of the surrounding rock mass and the cross-sectional shape of the anchorage. In typical applications, conservative failure modes have been applied to the design of tunnel-type anchorages (Park *et al*. 2009). Failure modes are typically reported to occur along the boundary surface of the adjacent rock mass parallel to the direction of the anchor load rather than in the form of a fan or wedge failure (Park *et al*. 2013, Park *et al*. 2014). Meanwhile, in Japan, the failure surface is

*Corresponding author, Ph.D.
E-mail: mkchung@kict.re.kr
[a]Research Specialist
E-mail: seunghwanseo@kict.re.kr
[b]Ph.D.
E-mail: hslim85@kict.re.kr

ISSN: 2005-307X (Print), 2092-6219 (Online)

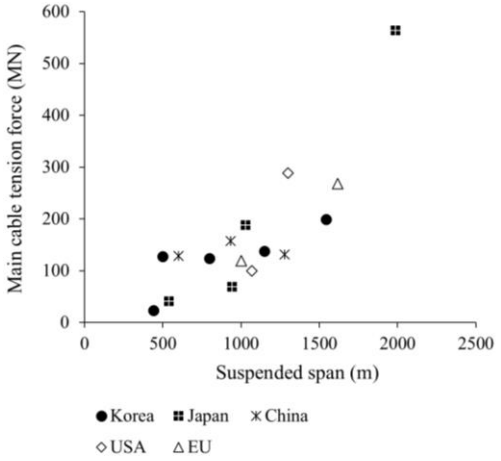

Fig. 1 Variation of main cable tension force with length of suspended span

assumed to form along the axial direction at the surface of the anchorage body. However, in practice, a wedge-shaped failure, which causes the surrounding ground to be pushed together, should typically be assumed when a stress is applied to the ground in the axial direction and the radial direction of the enlarged section (Kanemitsu *et al*. 1980).

The failure mechanism of the ground significantly affects anchorage design. However, because no design guidelines have been developed to date, the resulting anchorage design varies depending on the designers. The tunnel-type anchorage was applied to the Ulsan Grand Bridge based on the design methods and anchorage cross-sectional shape of the Shimotsui-Seto Bridge and Kurushima Kaikyo Bridge in Japan (Park *et al*. 2009, Kim *et al*. 2011). The Ulsan Grand Bridge is a tablet-type suspension bridge with a span of 1,150 m. Gravity anchorage is applied at the Eonyang side of the bridge, and a tunnel-type anchorage is applied to minimize the damage to the Yeompo mountain side (Fig. 2). The tunnel-type anchorage used in the Ulsan Grand Bridge was applied with a constant tunnel diameter (11 m). The tunnel was enlarged from the inside to avoid stress concentration on the rock and concrete and to widen the compression area generated in the rock. This constitutes a slight difference from the bridges constructed in the United States, Europe, and China. In this case, no specific experiments were performed on the failure mode to calculate the pull-out resistance of the anchorage.

In this study, we analyzed the pull-out behavior by replicating the anchorage shape and the surrounding rock mass of the Ulsan Grand Bridge via scaled model experiments considering the scale factor. We focused on the direct observation of the initial failure behavior and failure mode of the tunnel-type anchorage with respect to the pull-out load. Although the use of a 3-dimensional (3D) test improves the possibility of practical implementation, it presents difficulties in analyzing the measurement data when experiments are performed to measure the failure mode, initial deformation, and strength of the anchorage at failure. Therefore, the failure section was identified using 2-dimensional tests (2D), and then 3D tests can be performed based on these results.

The tunnel-type anchorage of the Ulsan Grand Bridge was simplified to investigate the pull-out behavior and failure patterns according to the main design parameters. In particular, model experiments were performed by varying the length of the anchor plate, the main structure of the tunnel anchorage, as well as the strength of the anchorage body material relative to the surrounding rock mass. In addition, the initial failure pattern was quantitatively analyzed via image analysis and compared with the observed failure results of the model experiments. Recently, image processing methods have been applied in various areas for advanced inspections and assessment in the geotechnical engineering field (Yu *et al.* 2014, Altunbas *et al.* 2017, Jeong and Jeon 2018, Fei *et al.* 2019). This study discussed the possible failure modes of the tunnel-type anchorage using the results of model experiments, which can be used as the basis for the estimation of failure modes and bearing capacity in tunnel-type anchorage design.

2. Materials and experimental methods

2.1 Scaled model test

The scaled model test is a typical method for investigating the stability of the ground and associated structures and visually represents physical and practical results. This constitutes an advantage compared to a numerical analysis. Therefore, the scaled model test represents a useful experimental method for the design of ground structures. However, a problem exists in that an appropriate model material to completely reproduce the rock mass at the target site does not exist.

In this model test, the shape of the tunnel-type anchorage was determined based on the design drawings of the Ulsan Grand Bridge, and all the conditions of the site were converted using a scale factor in dimensional analysis to reproduce site conditions, thereby yielding reliable results. In the scaled model test, a mixture of gypsum, sand, and water was used as the material for the model rock mass. Using the indoor physical property test, the mixing ratio of the model material was determined, and the strength of the actual anchorage relative to that of the surrounding rock mass was simulated considering the scale factor.

In previous studies, scaled model tests were conducted to examine the stability of hard rock tunnels, producing reliable results (Hobbs 1968, Jung and Kim 2006, Chung *et al*. 2013). In this study, the scale factor was determined in the same manner, as described below, and a series of model tests was subsequently performed.

In the scaled model test, the scale factor was calculated based on a dimensional analysis of the overall elements of the actual site. The physical properties of the local rock mass and the model test material were compared, and based on this, the tunnel-type anchorage of the Ulsan Bridge was reduced to design a model using appropriate model materials. When the three basic dimensions are length [L], mass [M], and time [T], the scale factor is calculated by first determining the scale factor for the length, and then using it to reduce the scale factors for time, density, mass, stress, etc. (Hobbs 1969).

(a) Actual view

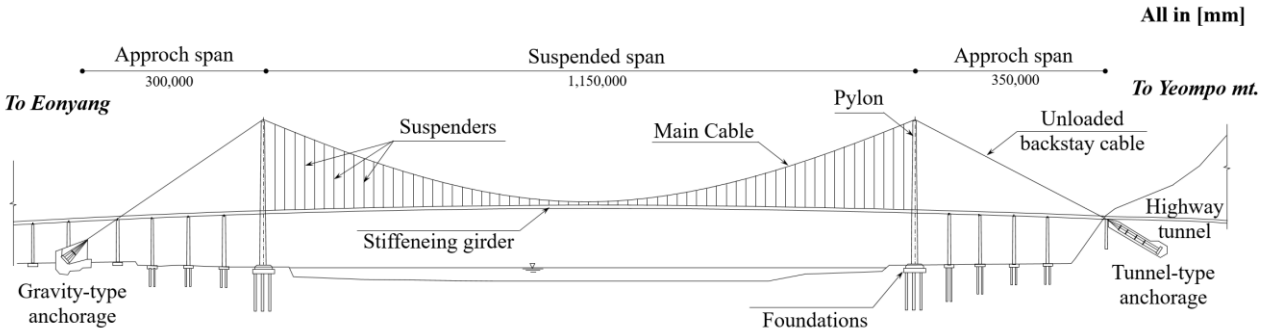

(b) Schematic diagram

Fig. 2 The Ulsan Grand Bridge

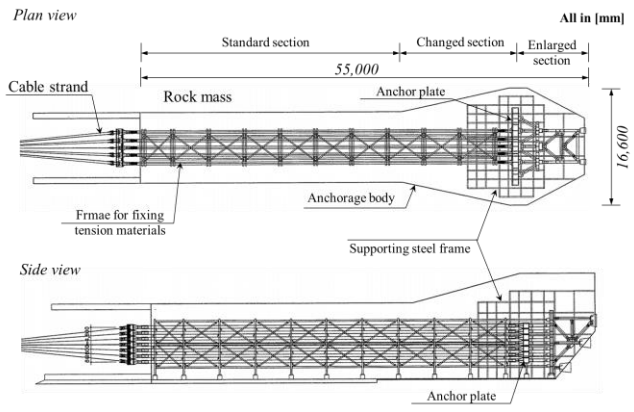

(a) Design drawing of the actual tunnel-type anchorage (Yooshin Co., Ltd. 2010a)

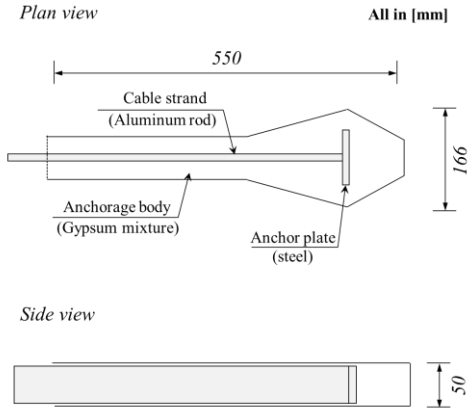

(b) Simplified shape for the model test

Fig. 3 Plan and side view of the tunnel-type anchorage body

Table 1 Scale factors used in the model tests, calculated by comparison with the actual design of the Ulsan Grand Bridge

Physical properties	Dimension	Scale factor
Length	[L]	1/100
Time	[T]	1/10
Density	$[ML^{-3}]$	1/1.75
Mass	[M]	$1/(1.75 \times 10^{6})$
Acceleration	$[LT^{-2}]$	1
Strength	$[ML^{-1}T^{-2}]$	1/174
Young's modulus	$[ML^{-1}T^{-2}]$	1/174

The scale factor for the length was determined as 1/100 considering the maximum size of the model specimen, and the size of the tunnel model and on-site tunnel-type anchorage. Next, the scale factor over time [T] was determined, where the concept of constant gravitational acceleration was used. In other words, because the field and laboratory measurements of the gravitational acceleration [LT-2] were the same, the scale factor for time [T] was 1/10

according to Eq. (1).

$$\frac{L}{T^2} = 1 \tag{1}$$

Applying the average density of the model material (sand, gypsum mixture) as 1.55 g/cm^3 and the average density of the target ground as 2.7 g/cm^3, the scale factor for density [ML-3] was calculated using Eq. (2)

$$\frac{M}{L^3} = \frac{1.55}{2.7} = \frac{1}{1.75} \tag{2}$$

On the other hand, because the scale factor for length [L] was 1/100, the scale factor for mass [M] in Eq. (2) was calculated as shown in Eq. (3).

$$M = \frac{1}{1.75} \times L^3 = \frac{1}{1.75} \times \left(\frac{1}{100}\right)^3 = \frac{1}{1.75 \times 10^6} \tag{3}$$

The scale factor of the three basic dimensions, length [L], time [T], and mass [M], were determined as described above, thus completing the basic dimensional analysis of this experiment. Additionally, the scale factor for properties such as stress, modulus of elasticity, and strength [ML^{-1}T^{-2}] was calculated using Eq. (4).

$$\frac{M}{LT^2} = \frac{\frac{1}{1.75 \times 10^6}}{\frac{1}{100} \times \left(\frac{1}{10}\right)^2} = \frac{1}{174} \tag{4}$$

Table 1 shows the result of the dimensional analysis, and summarizes the scale factors of this scaled model experiment for the actual Ulsan Bridge site. The length, mass, time, and density corresponded to the calculated scale factor, and Young's modulus was included in the range of physical properties that appear in the hard rock area when considering the scale factor and the value of the model material. In the case of strength, the theoretical scale factor was 1/174, giving the target strength of 1.03 MPa. However, the experiment is difficult to perform with a very small strength. Hence, a material with strength of 1.1 MPa, which is close to the target strength, was used.

In addition, the cable bundle inside the tunnel-type anchorage sphere was originally fixed to the anchor plate, but in the miniature model test, aluminum was used to sufficiently transmit the force without deformation against the pull-out load. The determined scale factors are shown in Table 1.

An illustration of the tunnel-type anchorage body is shown in Fig. 3(a); its structure is designed to transmit the cable tension of the suspension bridge to the inner anchor plate through a strand-and-tension frame. In this study, the frames of the fixing tension material and supporting steel frame, which do not serve as load-carrying structures, were excluded from the model test design. Instead, the aluminum cable strand and steel anchor plate were designed to a T-shape to simplify the model test (Fig. 3(b)).

The test was thus designed as a simplified version of the tunnel-type anchorage of the Ulsan Grand Bridge, which is installed in the direction of inclination on the hard rock slope into the anchorage installed in the vertical direction on the horizontal surface of rock mass without joints. In addition, because the behavior may vary depending on the shape of the changed section and enlarged section of the tunnel, the shapes of specimens were designed to effectively have the same shapes as the real sections to enhance the reliability of the model test (Fig. 3(b)).

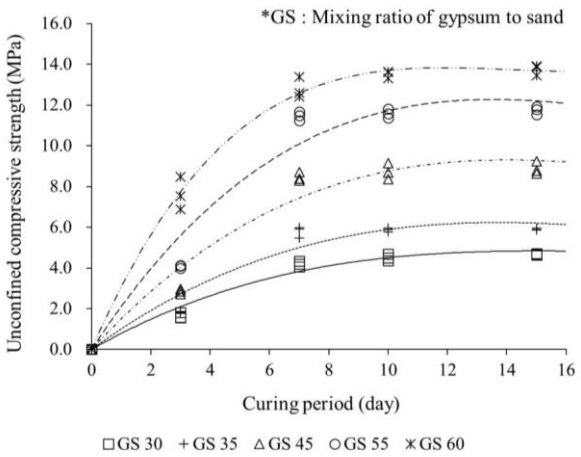

Fig. 4 Unconfined compressive strength of gypsum mixtures with curing time where GS is the ratio of gypsum to sand (wt%)

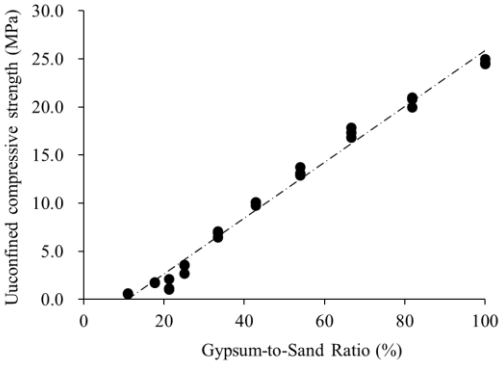

(a) Unconfined compressive strength

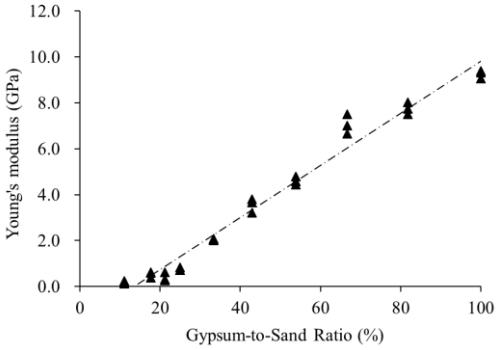

(b) Young's modulus

Fig. 5 Relationship between the physical properties and gypsum-to-sand ratio

2.2 Model materials

A mixture of sand, gypsum, and water was used to fabricate the surrounding rock mass and anchorage body

Table 2 Mixing ratio of the materials in the model test

Model	Mixed ratio of model materials (wt%)			Density of rock mass		Strength (MPa)
	Gypsum	Sand	Water	In-situ (kN/m^3)	Model material (kN/m^3)	
Surrounding rock mass	12	49	23	27	15.5	0.5
Anchorage body	8	57	23			1.1

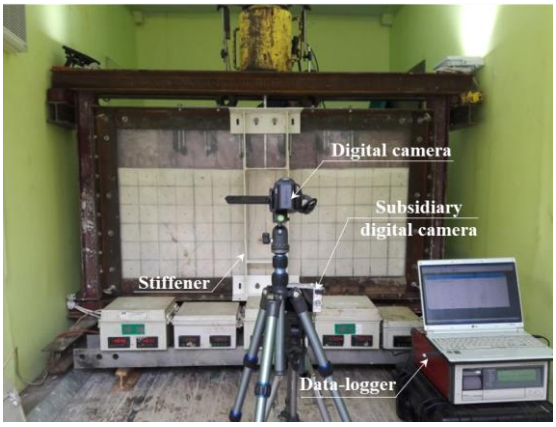

(a) Photo

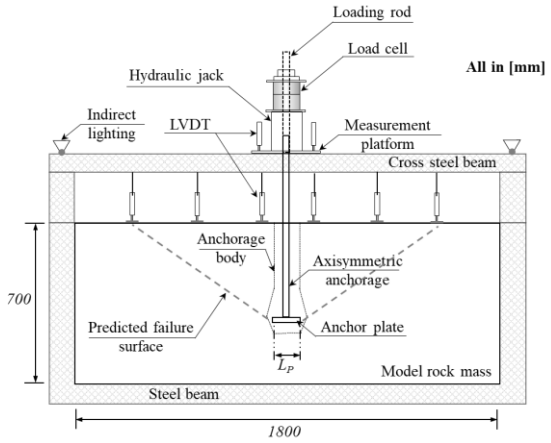

(b) Schematic

Fig. 6 General view of test setup

Table 3 Model test case conditions

Test ID	Anchor plate length L_p (mm)	Property ratio r* (m_T/m_R)	Pull-out direction	Anchorage body shape
C-1	110	0.5	Upward vertical	Symmetric
C-2	110	0.5		
C-3	110	0.25		
C-4	110	0.75		
C-5	73	0.5		
C-6	73	0.5		

r* represents the ratio of the compressive strength of the tunnel-type anchorage body (m_T) to the compressive strength of the rock mass (m_R)

materials. These materials have been widely used in scaled model tests to simulate rock masses and can achieve various strengths according to the mixing ratio by weight (Coquard and Boisetelle 1994). To determine the mixing ratio of the model rock mass, an indoor property test was conducted by changing the sand/gypsum/water mixing ratio while maintaining the total weight of the mixture. The sand used was Jumunjin standard sand (K.S.L. 5100), and Hi CAST+(CH) gypsum was obtained from Mungyo Gypsum & Engineering. Three cylindrical specimens 5 cm in diameter and 10 cm in length were fabricated for the gypsum mixtures with various mixing ratios and dried for seven days to ensure that there were no changes in physical property values with respect to curing time (Fig. 4). Then, uniaxial compression tests (KS E 3033) and tensile strength tests (ASTM D 3967) were performed when the unit weight of each specimen was approximately 1.5 gf/cm^3. The results of the physical property test, which were analyzed using linear regression analysis, showed that the compressive strength and deformation modulus were significantly correlated with the gypsum/sand mixing ratio (Fig. 5). Meanwhile, when the proportion of gypsum was low, the actual physical properties of the rock mass could hardly be simulated, and the uniform physical properties could not be reproduced because of the high moisture content, which can considerably affect the accuracy of the test. Strength ranging from 0.5 to 1 MPa was required to match the scaled physical properties of the model rock mass and anchorage model materials. However, the strength range of approximately 0.5 to 1.1 MPa was used according to the aforementioned constraints. The mixing ratios of sand, gypsum, and water used for the composition of the model rock mass and anchorage body materials are summarized in Table 2 (Yooshin Co., Ltd. 2010b).

2.3 Test method

The model rock mass used in the scaled model tests was manufactured according to the principles of physical similarity with dimensions of 1,800 mm (width) × 700 mm (height) × 50 mm (thickness), which correspond to about 1/100 of the actual dimensions. The gypsum mixture used as the model material was mixed using a stirrer and slowly injected into the prepared test mold, and a 0.1 mm thick acrylic vinyl was attached to the inside of the mold to minimize the damage to the surface of the model specimen and wall friction during pull-out. After the mixture placement was completed, curing was performed at a constant temperature of 25°C for 7 days.

In this study, a plane strain state was required so that

deformation did not occur in the anchorage thickness direction during the 2D model tests of the tunnel-type anchorage. To directly observe the failure behavior, a 3 cm thick acrylic sheet was used on the front surface. An H-shaped reinforcement material was installed on top, which served as a stiffener (Fig. 6) to suppress the deformation in the frontal direction. Because of the characteristics of the 2D test, a limit was imposed on the implementation of the plane strain state. The pull-out behavior according to changes in the size of the anchorage plate was investigated. The types of the model test are shown in Table 3. Note that C-1 and C-2 share the same conditions, as do C-5 and C-6 repeated experiments.

For the pull-out tests, a load was applied using a displacement rate of approximately 2.0 mm/min until failure of the model rock mass. In the case of suspension bridge cable anchorages, the pull-out speed of the test was relatively high considering the load transfer process during construction and after operation (Yooshin Co., Ltd. 2010a). Pull-out load tests of soil and pile foundations are typically conducted at 0.5–1.0 mm/min (ASTM D 3689). In pull-out load test of concrete and metal structures, the test time was 14–33 s when the ultimate load was 10 kN and 29–67 s when it was 20 kN (ASTM C900-06). In this study, the anchorage of the gypsum mixture and aluminum was closer to the latter case. Accordingly, the load was applied at the above speed in accordance with the ASTM C900-06. The displacement volume was measured by installing linear variable differential transformers (LVDTs) at uniform intervals in the vertical direction on the upper part of the model rock mass, and the stress–strain relationship of the model rock mass was obtained by measuring the load acting on the rock mass through a load cell installed on the loading plate. In addition, grids and tracking points were marked at 10 cm intervals on the surface of the model rock mass after placement to facilitate the observation of its deformation. The overall experimental setup is shown in Fig. 6(b). The cracks on the surface were manually marked after the pull-out test.

3. Image processing technique and methodology

3.1 Image processing

3.1.1 Image acquisition

While recording images, a large amount of noise is generated on the surfaces because of the influence of the surrounding environment, necessitating an image pre-processing method. To provide image analysis after pre-processing, binarization and morphological techniques were performed to detect the cracks in the model rock mass (Ammouche *et al*. 2000, Ito *et al*. 2002, Lee *et al*. 2007, Otsu 1979). To investigate the failure behavior, the pixel difference method and the method of tracking specific points were applied (Ilsever and Unsalan 2012). Image acquisition and pre-processing proceeded as follows, using Mathematica as the image processing tool.

The 2D pull-out tests were performed indoors to minimize the influence of the surrounding environment. Indirect lighting was used to ensure that the illumination

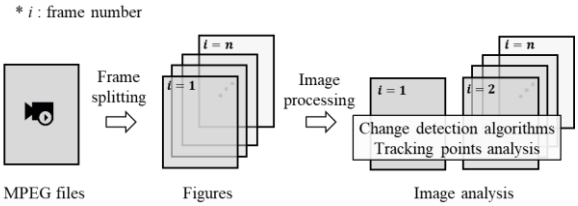

Fig. 7 Image processing flow chart

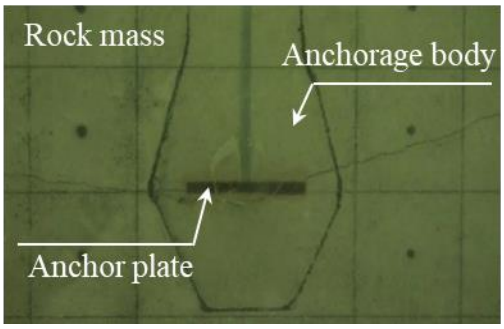

(a) Original image

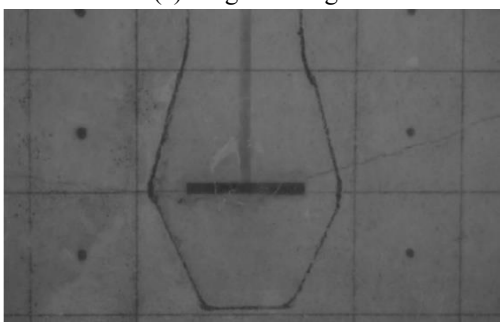

(b) Gray-scaled image

(c) Thresholding and binarized image

(d) Extra thresholding image

Fig. 8 Image processing example

was as constant as possible. An entry-level Sony HDR-CX500 digital camera was used to capture a frame size of

1440×1080 at a frame rate of 29.97 fps. The camera was on a tripod to ensure that the images were acquired at the same position without blurring, and the entire sequence of the experiment was also captured using a secondary digital camera. As shown in Fig. 7, images for each frame were extracted from MPEG files, and each image was subjected to pre-processing and subsequent analysis.

3.1.2 Gray scale

First, the multichannel image was converted to grayscale to simplify image processing, as shown in Fig. 8(b). Grayscale images are often used for image analysis because of their low complexity. This also eliminates the heterogeneity of the image due to illumination through shading correction.

3.1.3 Thresholding and binarization

The shaded image was converted into a binarized image using a fixed threshold value. With fixed thresholds, it was difficult to identify cracks in the central section of the anchorage body and cracks occurring in the rock mass. Therefore, the threshold was adjusted locally to allow identification of these structures, as shown in Fig. 8(c) (Rosin and Loannidis 2003).

3.1.4 Extra thresholding and morphological structure extraction

Additional correction was performed to extract the morphological structure of the cracks. When a section with cracks was binarized, as shown in Fig. 8(b), the black dots around the cracks could be recognized as a crack as well. Therefore, the threshold value was additionally adjusted to correct for these regions, as shown in Fig. 8(c). In this state, the morphological structure of cracks was extracted, and cracks were recognized, as shown in Fig. 8(d). Through this process, the final morphological shapes were recognized as cracks and used for image analysis, as shown in the example in Fig. 9.

3.2 Change detection algorithms

After pre-processing the entire series of images, we applied image differencing algorithms to analyze the changes in the images over time. Image differencing is a very commonly used algorithm that subtracts one image from another pixel by pixel and determines a certain threshold (differentiating between change and no change) to detect changes (Lu *et al*. 2004, Liu *et al*. 2004, Li and Yeh 2004).

Let us denote Frame 1 and Frame 2 as the acquired images in the model test, where Frame 2 is the more recent image. Let X denote the image from Frame 1 and Y the image from Frame 2. Let x_{ij} denote the pixel value in image X, and y_{ij} denote a pixel value in image Y. The difference d_{ij} is given by

$$d_{ij} = y_{ij} - x_{ij} \quad (5)$$

where i and j denote the line order and column order of the subject pixel. The selection of a threshold is problematic in image differencing, and several methods have been developed accordingly. Assuming a Gaussian distribution, the changed pixels are found in the tails of the distribution and unchanged pixels are found around the mean. Therefore, one method selecting a change threshold uses the standard deviations from the mean, whereas in another method, the analyst decides the threshold interactively and reviews the result on screen (Singh 1989).

Fig. 9 Example of sequence for morphological determination of cracks

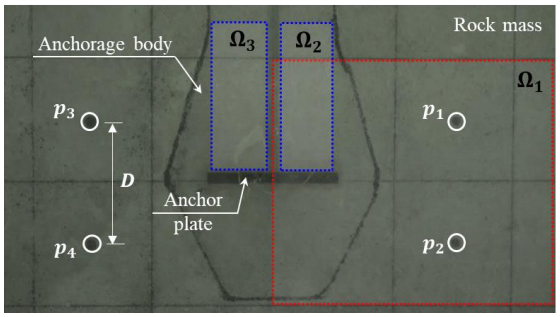

Fig. 10 Definition of calculation area for image analysis (where Ω_1 indicates the area for observing crack propagation; Ω_2, Ω_3 indicate the area for observing failure inside anchorage body; and $p_1 - p_1$ are tracking points)

Image analysis was performed using the pre-processed images described previously, and the results were analyzed for the areas shown in Fig. 10. The Ω_1 region was used to investigate the propagation of cracks. The cumulative pixel variation in regions Ω_2 and Ω_3 was investigated to observe the extent of failure in the anchorage body. The thickness of the cracks was measured in units of pixel number by calculating the changes in the distance (D) between the tracking points of each frame.

4. Experimental results

4.1 Failure mode and crack pattern

The final crack patterns obtained from the pull-out tests are shown in Fig. 11. Tests C-1 and C-2 applied the same geometric and mechanical reduction ratios as the actual tunnel-type anchorage of the Ulsan Grand Bridge, with the results shown in Figs. 11(a) and 11(b).

In both tests, failure was initiated at both ends of the anchor plate, and the final failure mode exhibited a wedge shape. Failure patterns could also be identified in the heaving displacements of the model rock mass surface. In Fig. 12, the value in the middle at 0 mm represents the displacement of the anchorage, where an initial elevation can be observed to have occurred. Finally, failure appeared as shown in Fig. 12(a). This tendency was also observed in Fig. 12(b), which represents C-2.

In C-3 and C-4, the ratio (r) of the compressive strength

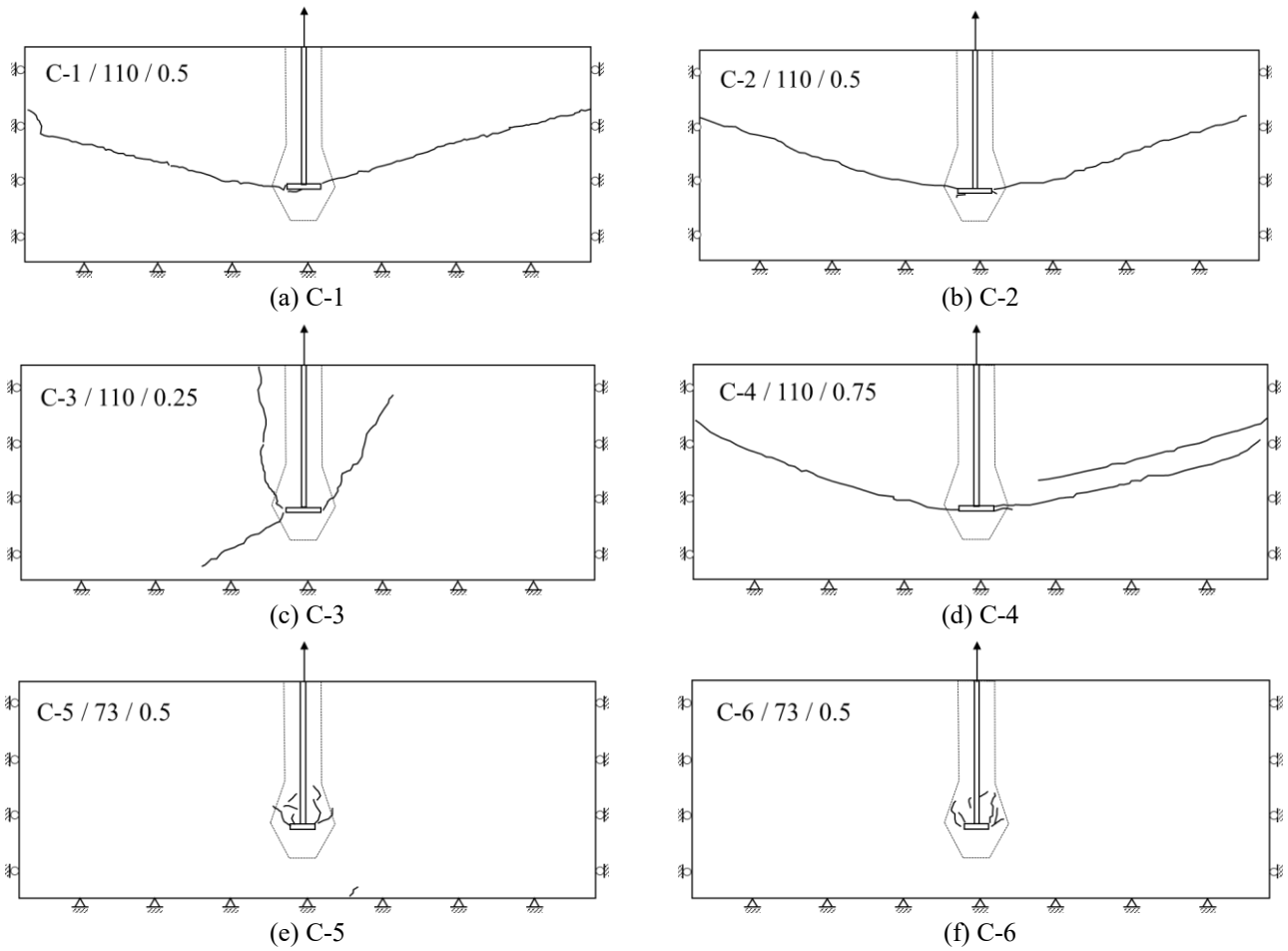

Fig. 11 Failure pattern of the scaled mode test where upper left label represents test ID/anchor plate length/property ratio

of the anchorage body material to that of the rock mass were varied by holding the physical properties of the surrounding rock mass constant and varying only the properties of the anchorage body material. In C-3, the anchorage body material was 25% of the strength of the surrounding rock mass, and in C-4, it was 75%. For C-3, like for C-1, microcracks were initially generated at the bottom of the anchor plate, causing pieces to fall out of the anchorage body material, eventually destroying it. Compression fracture occurred inside the anchorage body, and cracks were transferred to the surrounding rock mass at the changed section of the anchorage body. In general, failure was not in the form of a wedge but was rather similar to the pull-out failure mode. In contrast, for C-4, the final failure was of the wedge type. However, even in this case, the initiation of destruction occurred near the anchor plate, from where the cracks spread to the surrounding rock mass.

This form of destruction was similar to that for C-1 and C-2. In terms of the heaving displacement of the model rock mass surface in C-3, the heaving occurred only where the anchorage cable was installed, and there was no displacement in the model rock mass. The heaving displacement of the model rock mass surface in C-4 was also similar to that of C-1 and C-2. The conditions for C-5 and C-6 were the same as for C-1 and C-2, except the length of the anchor plate (L_p) was smaller than the tunnel diameter. In both cases, the final failure pattern was of the pull-out type. In the initial stages, failure occurred at both ends of the anchor plate in all cases. Both C-5 and C-6 indicated that the cracks were not transferred to the surrounding rock mass, but compressive failure occurred continuously inside the anchorage body. This trend can also be observed in Figs. 12(e) and (f), and only the anchorage cable was displaced according to the tensile load.

4.2 Load-displacement curve

The tensile load-displacement curves of the tested tunnel-type anchorage models are shown in Fig. 13. To identify the failure behavior, the curves are grouped according to failure mode: Fig. 13(a) shows the results for the wedge failure mode and Fig. 13(b) shows the results for the pull-out failure mode. For the wedge-shaped failures of C-1 and C-2 in Fig. 13(a), the tensile load up to about 10 kN indicates localized failure and is close to the elastic region. The development of the failure can be observed as the materials yield. The maximum tensile load of 11.5 kN was found to occur at displacements in the range of 5 to 10 mm, which increased with the residual resistance without increasing the magnitude of the maximum tensile load itself. Test C-4 exhibited an increase in the strength of the

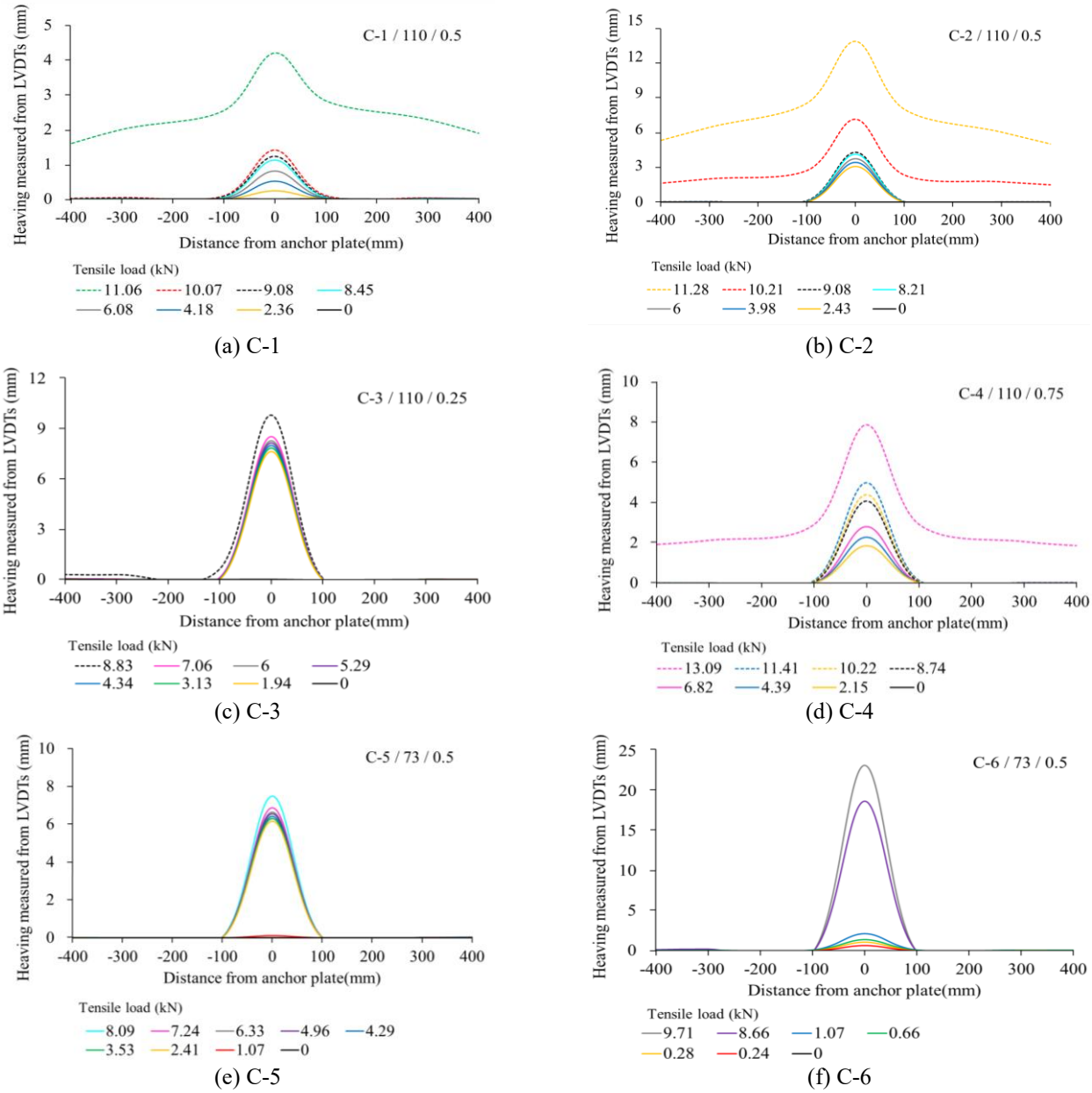

Fig. 12 Heaving measured from LVDTs in the scaled mode test where upper right label means test ID/anchor plat length/property ratio

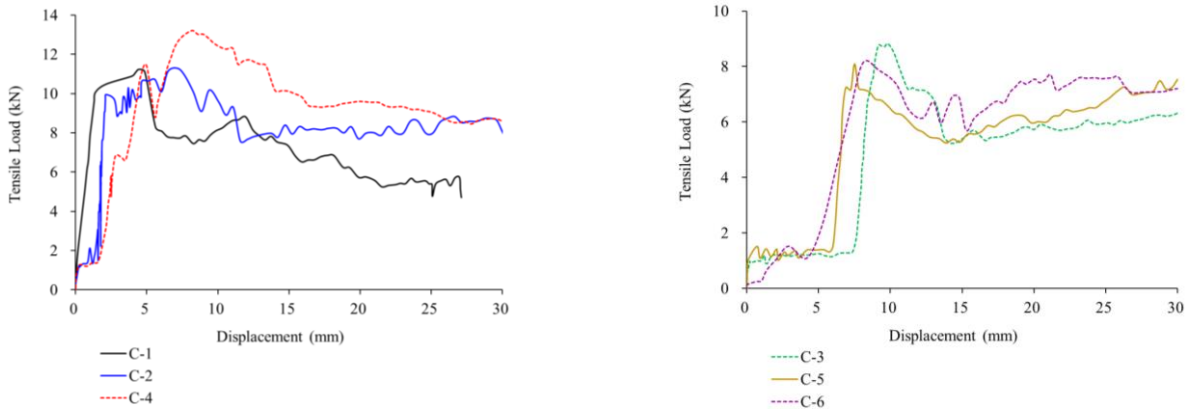

Fig. 13 Tensile load–displacement curve for model test

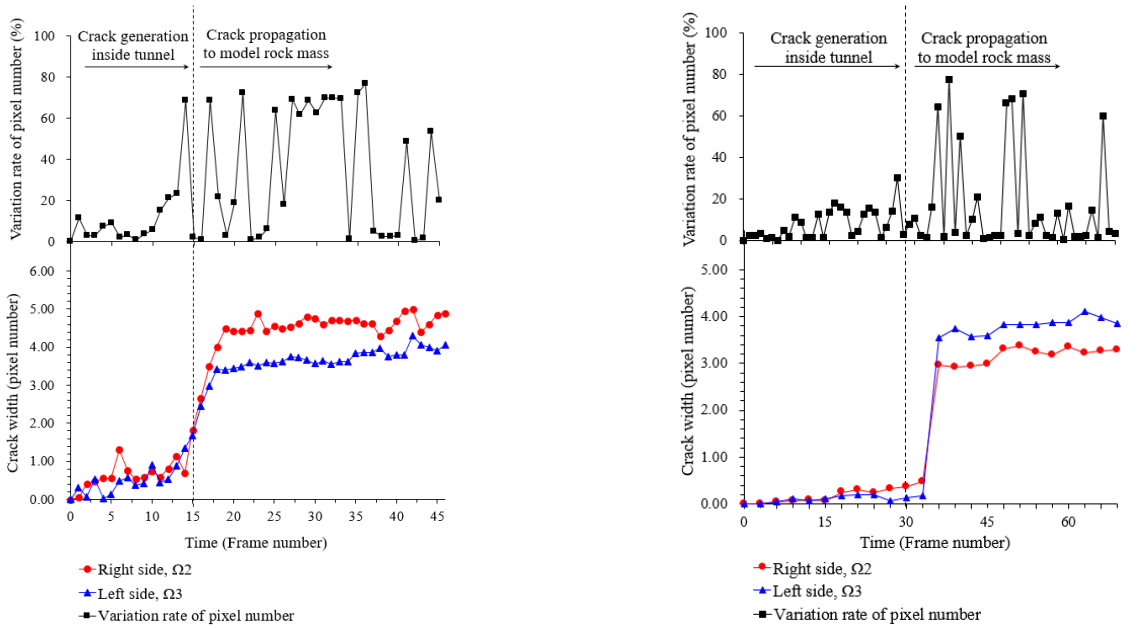

(a) C-1 (b) C-4

Fig. 14 Pixel variation and crack thickness for wedge failure mode

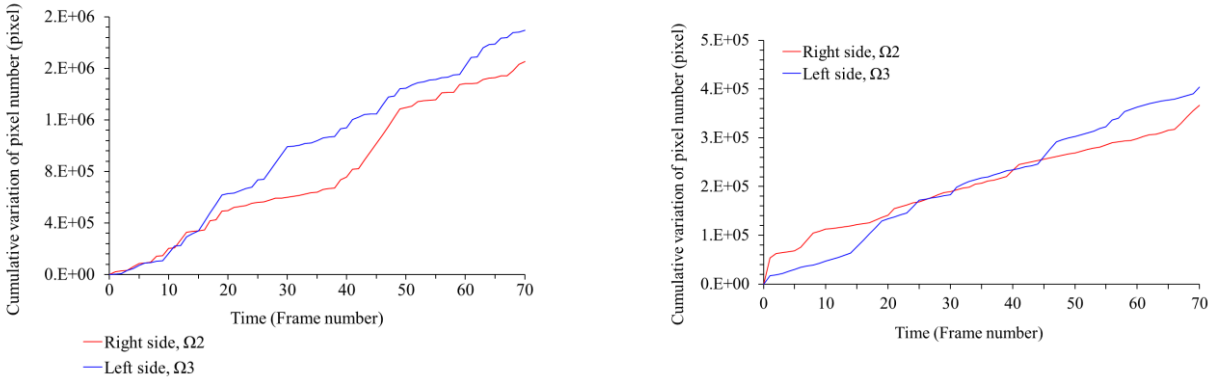

(a) C-5 (b) C-6

Fig. 15 Cumulative pixel variation curve for pull-out failure mode

anchorage body material, and the maximum tensile load was approximately 13 kN; the overall behavior was similar to that of C-1 and C-2.

Fig. 13(b) shows the results for the pull-out failure mode. Unlike for the wedge failure mode, the anchorage body material was compressed and destroyed up to a depth of 5-7 mm, and the displacement increased without a corresponding increase in the tensile load. After that, plastic failure occurred up to about 8–8.6 kN, and then, the displacement increased due to residual resistance without increasing the tensile load.

4.3 Image analysis for wedge failure mode

The failure of the model rock mass during the model tests often occurred in an extremely short time, and it was therefore not easy to investigate the initial failure behavior. Especially in the case of micro cracking at an early stage, it is often difficult to analyze sequentially recorded images. Therefore, to observe the crack transition, the pixels corresponding to sections of morphologically determined cracks were examined frame by frame, and the variations between each frame were investigated. Fig. 14 shows the pixel variation and the distance (D) between tracking points for each frame using the change detection method discussed in Section 3.1. For C-1, starting at about the 15th frame, failure occurred in the anchor plate and anchorage body, and then rapid pixel changes occurred because of the cracking of rock mass. From the variation in the pixel number, it can be assumed that cracks first propagated into the rock mass after the initial failure in the vicinity of the anchor plate and along the tunnel. Thereafter, a constant tensile load was applied, and the variation in pixel number was continuously increased. Fig. 14(b) shows the results of C-4 when the properties of the anchorage body and rock mass are different. In this case, the wedge-type failure was also observed, and it can be deduced that the failure propagation progressed into the rock mass near the anchor

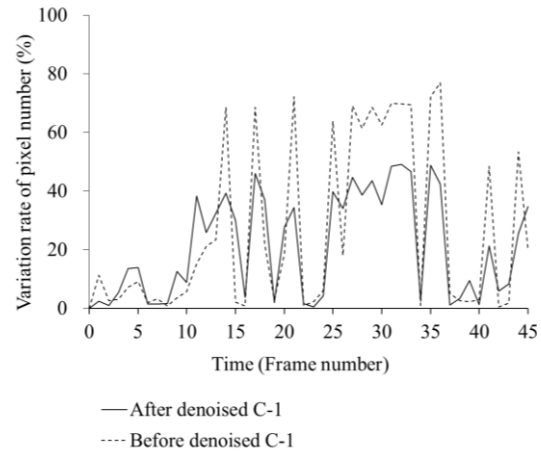

(a) C-1

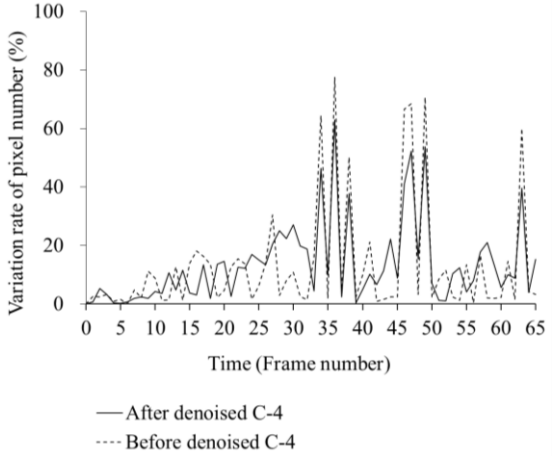

(b) C-4

Fig. 16 Comparison of pixel variation before and after noise reduction using the median filter

plate and along the tunnel. The failure pattern resembled that of C-1.

When the wedge-type failure occurred, the failure patterns on the left and right side of the rock mass were different. Both C-1 and C-4 exhibited the same wedge-type failure, but the failure patterns in the rock mass were slightly different. To compare the failure extent, the coordinates of the tracking points marked on the model rock mass were extracted and the distances between the two points were calculated. As cracks occur, the distance (D) changes, so the thickness of the cracks between tracking points can be measured in units of pixels. We investigated the failure patterns of the left and right rock mass at a given distance from the anchor plate. The crack thicknesses estimated by tracking the coordinates of p_1–p_4 are shown in the bottom graph of Fig. 14. As shown in Fig. 14(a), failure occurred where the thickness of the crack increased sharply. The failure extent of the left- and right-side rock masses were compared over time. In the case of C-1, the cracks in the right-side rock were thicker, and in C-4, the cracks in the left-side rock were thicker. Therefore, even a rock mass with the same composition exhibited different extents of failure in the left and right sides of the rock mass, likely because of the non-uniformity of the mixed materials.

4.4 Image analysis for pull-out failure mode

When the tunnel-type anchorage fails in accordance with pull-out failure mode, the failure effect does not reach the rock mass, and the anchorage body materials are compressively broken. The results of C-5 and C-6 represent the pull-out failure mode. In this case, the total failure behavior was considered by examining the cumulative pixel variation rather than comparing the pixel variation between each frame. Fig. 15 shows the cumulative pixel variation for two regions (Ω_2 and Ω_3). At the beginning of failure, the stress was concentrated in the vicinity of the anchor plate, so that the cumulative pixel variation of the two regions was similar, but the variation in pixel region Ω_2 increases over time. Thus, even under the same tensile loading, the extent of failure in the anchorage body was different and could be validated quantitatively through the cumulative variation in the pixel number.

4.5 Difference in pixel variation due to removing noise

To minimize the noise in the collected images, a median filter was applied during pre-processing. The median filter is advantageous in that the deterioration of the edge is relatively small among the nonlinear filtering algorithms (Cho *et al*. 2010, Pratt 1978), and edge detection is important for identifying cracks. As shown in Fig. 16(a), for C-1, after the noise was removed using the median filter, the number of pixels counted was lower, but the tendency is similar (though it exhibits slight differences in relative magnitude). It is thus considered that the application of the median filter increased the detection rate of initial fine cracks.

In addition, the results of denoising the data for C-4 using the median filter show a similar tendency (Fig. 16(b)). Thus, even if the failure mode cannot be observed with the naked eye because of the influence of the measurement equipment or experimental environment, it is possible to quantitatively evaluate failure propagation using the image processing-based method proposed in this study.

5. Discussion

5.1 Effect of anchor plate length

In the model test, the size of the anchor plate (L_p) was tested by applying 110 mm with the same reduction ratio as the actual Ulsan Grand Bridge and 73 mm which is smaller than the tunnel diameter. As the size of the anchor plate decreased, the ultimate tensile load decreased (Fig. 13). When the L_p was 110 mm, wedge-type failure occurred because of the compression fracture and tension crack transition of the anchorage body (Fig. 17(a)). However, as C-3 in Fig. 17(a), when the difference (r) in material properties between the tunnel material and the surrounding rock mass was less than 0.5, it was close to pull-out type failure. When L_p was 73 mm, the anchorage body underwent compressive failure but tensile crack was limited in the material inside the tunnel (Fig. 17(b). The final failure mode depends on the length of the anchor plate, and

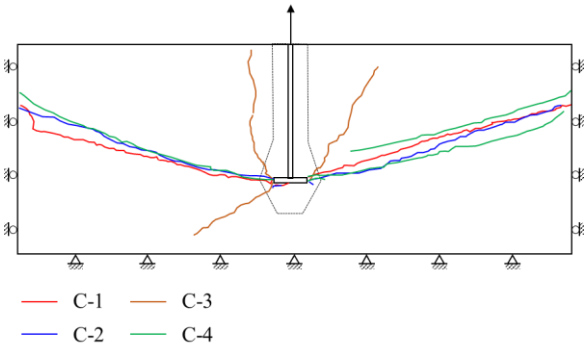

(a) L_p 110 mm

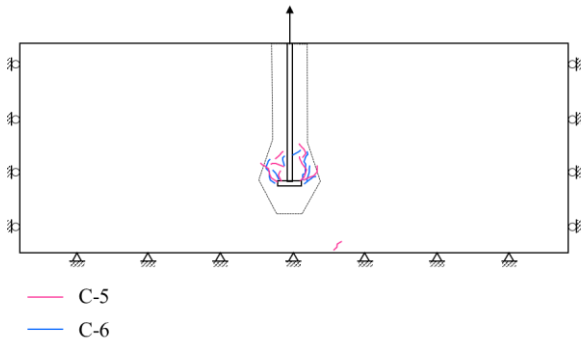

(b) L_p 73 mm

Fig. 17 Failure pattern with changes in anchor plate length

if L_p is smaller than the diameter of the standard section of the tunnel, it would be reasonable to assume a pull-out failure mode. Therefore, the anchorage size is considered to be the main variable to determine the failure mode in the design of anchorage.

5.2 Effect of variation in material properties

As the ratio of the compressive strength of the anchorage body to that of the model rock mass increases, the ultimate tensile load of the anchorage also increases. This can be seen from the results in Fig. 13. Pull-out failure occurred when the compressive strength of the anchorage body material was 25% stronger than that of the surrounding rock mass. Upward displacement was concentrated only in the anchorage body because of the tensile cracking inside the tunnel. In this case, in an actual tunnel-type anchorage, the ultimate tensile resistance would be determined by the shear resistance at the interface between the anchorage body and the surrounding rock mass. In addition, when the compressive strength of the anchorage body material was more than 50% stronger than that of the surrounding rock mass, the tensile cracks initiating from the anchor plate were transferred to the surrounding rock mass. Thus, the failure was wedge-shaped, and the upward displacement distribution of the model rock mass was accordingly observed to have a wedge shape.

5.3 Detecting failure mode through image analysis

By analyzing the results of the changes in detection method and the tracking point together, we can understand the initial failure behavior of tunnel-type anchorage. Fig. 14(a) shows the changes in pixel variation and the crack thickness through point tracking in the case of C-1. Starting from the 15th frame, it can be divided into destruction of the rock inside and around the tunnel. Prior to the 15th frame, there was no change in the distance between points in the model rock, but there was a sharp change in the amount of pixel change. This means there was no change in the surrounding rock mass and the destruction within the tunnel. From 15 frames onwards, the distance (D) between tracking points increased rapidly, and the cracks were continuously propagated. Fig. 14(b) shows the changes in pixel variation and crack thickness frame by frame for C-4. In this case, it can be divided into the destruction of the rock inside and around the tunnel starting from the 30th frame. Prior to the 30th frame, there was no change in the distance between the points of the model rock, but there were several changes in the number of pixels. The destruction inside the tunnel affected the amount of pixel variation. After the 30th frame, the crack suddenly increased, the distance between the two points increased, and the amount of pixel variation also changed steadily. In the case of C-4, there was a small difference in strength between the tunnel and the surrounding rock mass, and it can be seen that the crack developed rapidly due to the changes in the distance (D) compared to the C-1.

6. Conclusions

To analyze the characteristics of the failure behavior of a tunnel-type anchorage, a series of scaled model tests were conducted using the 2D model tests focused on the initial failure behavior and the direct observation of failure mode. Experiments were performed by varying the shape of the main structure of the anchorage and the properties of the anchorage body. In addition, failure behavior was quantitatively analyzed using image analysis. The main conclusions of this study are as follows:

(1) As a result of the scaled model tests simulating the tunnel-type anchorage of the Ulsan Grand Bridge, the final failure mode was found to be of wedge type. In addition, the results of the image analysis showed that the initial failure pattern due to the tensile load occurred when cracks initiated in the section of the anchorage body in contact with the lower section of both ends of the anchor plate. The cracks generated at both ends of the anchor plate were then transferred to the surrounding rock mass through the anchorage body and finally manifested as a wedge-shaped failure mode.

(2) The failure mode was observed to change according to the length of the anchor plate, which is the main structure of the tunnel-type anchorage. If the length of the anchor plate (L_p) was larger than the diameter of the standard section of the tunnel, the failure mode was wedge-shaped, whereas if L_p is smaller, the failure mode was of the pull-out type. L_p is a major parameter determining failure mode.

(3) The failure pattern changed according to the ratio (r) of the compressive strength of the anchorage body material

to that of the surrounding rock mass. If r was greater than 0.5, a wedge failure mode was observed, otherwise a pull-out failure mode was observed.

(4) Two-dimensional model experiments could be applied in a quantitative analysis using the image change detection method and point tracking. In particular, even if there is no pattern of the model material or expensive photography equipment, a quantitative analysis is possible using the pixel difference method and point tracking.

(5) The scaled model tests conducted in this study provided meaningful results by analyzing the failure mechanism through direct observation of initial failure behavior inside the tunnel-type anchorage, and can thus be used as basic data to inform more reasonable tunnel-type anchorage design.

Acknowledgments

This research was supported by a grant (20SCIP-B119947-05) from Construction Technology Research Program funded by Ministry of Land, Infrastructure and Transport of Korean government.

References

Altunbas, A., Soltanbeigi, B. and Cinicioglu, O. (2017). "Determination of active failure surface geometry for cohesionless backfills", *Geomech. Eng.*, **12**(6), 983-1001. https://doi.org/10.12989/gae.2017.12.6.983.

Ammouche, A., Breysse, D., Hornain, H., Didry, O. and Marchand, J. (2000), "A new image analysis technique for the quantitative assessment of microcracks in cement-based materials", *Cement Concrete Res.*, **30**(1), 25-35. https://doi.org/10.1016/S0008-8846(99)00212-4.

ASCE (1979), "Long span suspension bridge: History and performance", *Proceedings of the ASCE National Conventions*, 109-127, Boston, MA, USA.

China Communication Press (2015), Industry Standard Editorial Committee of the People's Republic of China. Design Specification for Highway Suspension Bridge, Beijing, China.

Cho, D.R., Song, J.M. and Lee, D.H. (2010), "An adaptive noise reduction method using noise and edge information for Gaussian-noise images", *J. Eng. Technol.*, **20**, 61-69.

Chung, J.S., Moon, I.K. and Yoo, C.H. (2013), "Behavior characteristics of tunnel in the cavity ground by using scale model tests", *J. Kor. Geo-Environ. Soc.*, **14**(12), 61-69. https://doi.org/10.14481/jkges.2013.14.12.061.

Coquard, P. and Boisetelle, R. (1994), "Water and solvent effects on the strength of set plaster", *Int. J. of Rock Mech. and Min. Sci.*, **31**(5), 517-524. https://doi.org/10.1016/0148-9062(94)90153-8.

Dakeuchi, K.O. and Yoshida, Y.T. (1984), "Tunnel type anchorage", Construction report of Honshousikoku connection bridge, Research Report No. 22(11).

Fei, S., Tan, X., Wang, X., Du, L. and Sun, Z. (2019). "Evaluation of soil spatial variability by micro-structure simulation", *Geomech. Eng.*, **17**(6), 565-572. https://doi.org/10.12989/gae.2019.17.6.565.

Han, Y., Liu, X., Wei, N., Li, D., Deng, Z., Wu, X. and Liu, D. (2019), "A comprehensive review of the Mechanical behaviour of suspension bridge tunnel-type anchorage", *Adv. Mater. Sci. Eng.*, 3829281. https://doi.org/10.1155/2019/3829281.

Hobbs, D.W. (1968), "Scale model study of strata movement around mine roadways: I. the dependence of roadway closure upon rock strength", *Int. J. of Rock Mech. Min. Sci.*, **5**, 219-235. https://doi.org/10.1016/0148-9062(70)90011-2.

Hong, E.S., Cho, G.C., Baak, S.H., Park, J.H., Chung, M. and Lee, S.-W. (2014), "A numerical study on pull-out behavior of cavern-type rock anchorages", *J. of Korean Tunn. Undergr. Sp. Assoc.*, **16**(6), 521-531. https://doi.org/10.9711/KTAJ.2014.16.6.521.

Ilsever, M. and Ünsalan, C. (2012), *Two-Dimensional Change Detection Methods: Remote Sensing Applications* (Springer Briefs in Computer Science), Springer, London, U.K.

Ito, A., Aoki, Y. and Hashimoto, S. (2002), "Accurate extraction and measurement of fine cracks from concrete block surface image", *IEEE Industr. Electron. Soc.*, **3**, 2202-2207. https:// https://doi.org/10.1109/IECON.2002.1185314.

Jeong, H. and Jeon, S. (2018), "Characteristic of size distribution of rock chip produced by rock cutting with a pick cutter", *Geomech. Eng.*, **15**(3), 811-822. https://doi.org/10.12989/gae.2018.15.3.811.

Jung, H.R. and Kim, J.W. (2006), "Deformation behavior around tunnel in anisotropic rocks considering joint orientation and rock pressure condition using scaled model tests", *Kor. Soc. Rock Mech.*, **16**(4), 313-325.

Kanemitsu, H., Omachi, T. and Higuchi, K. (1980), "Calculation method of ultimated resisting pull strength of tunnel type of anchorage for suspension bridge", Honsi Technical Report.

Kim, K.W., Cho, N.S. and Na, Y.M. (2011), "Anchorage design of Ulsan Grand Bridge", *Mag. Concrete Inst.*, **23**(4), 51-54.

Lee, B.Y., Kim, J.K., Kim, Y.Y. and Yi, S.T. (2007), "A technique based on image processing for measuring cracks in the surface of concrete structures", *Proceedings of the SMiRT 19*, Toronto, August.

Li, X. and Yeh, A.G.O. (2004), "Analyzing spatial restructuring of land use patterns in a fast-growing region using remote sensing and GIS", *Landscape Urban Plan.*, **69**, 335-354. https://doi.org/10.1016/j.landurbplan.2003.10.033.

Li, Y., Luo, R., Zhang, Q., Xiao, G., Zhou, L. and Zhang, Y. (2017). "Model test and numerical simulation on the bearing mechanism of tunnel-type anchorage", *Geomech. Eng.*, **12**(1), 139-160. https://doi.org/10.12989/gae.2017.12.1.139.

Liu, Y., Nishiyama, S. and Yano, T. (2004), "Analysis of four change detection algorithms in bi-temporal space with a case study", *Int. J. Remote Sens.*, **25**(11), 2121-2139. https://doi.org/10.1080/01431160310001606647.

Lu, D., Mausel, P., Brondízio, E. and Moran, E. (2004), "Change detection techniques", *Int. J. Remote Sens.*, **25**(12), 2365-2407. https://10.1080/0143116031000139863.

Otsu, N.A. (1979), "A Threshold selection method from gray level histogram", *IEEE T. Syst.*, **9**(1), 62-66. https://doi.org/10.1109/TSMC.1979.4310076.

Park, C.S., Park, J.H., Chung, M.K. and Oh, I.K. (2013), "A study for improvement of suspension bridge's tunnel anchorage design", *Proceedings of the Korean Society of Civil Engineering Annual Conference*.

Park, C.S., Park, J.H. and Chung, M.K. (2014), "Recent study for improving the calculation method of ultimate pull-out resistance of tunnel anchorage", *Proceedings of the Korean Geotechnical Society Spring National Conference*, Seoul, Korea, March.

Park, J.W., Chung, S.T. and Cho, J.H. (2009), "The design of tunnel type anchorage in Ulsan Grand Bridge", Yooshin Technical Report, **16**, 328-336.

Pratt, W.K. (1978), *Digital Image Processing*, John Wiley and Sons, Inc., New York, U.S.A.

Rosin, P.L. and Loannidis, E. (2003), "Evaluation of global image thresholding for change detection", *Pattern Recogn. Lett.*, **24**(14), 2345-2356.

https://doi.org/10.1016/S0167-8655(03)00060-6.
Singh, A. (1989), "Digital change detection techniques using remotely-sensed data", *Int. J. Remote Sens.*, **10**(6), 989-1003. https://doi.org/10.1080/01431168908903939.
Yooshin Co., Ltd., (2010a), Ulsan Grand Bridge and Access Road Private Proposal Project, Basic Design Report.
Yooshin Co., Ltd., (2010b), Ulsan Grand Bridge and Access Road Private Proposal Project, Geotechnical Soil Report.
Yu, Q., Zhu, W., Tang, C. and Yang, T. (2014). "Impact of rock microstructures on failure processes - Numerical study based on DIP technique", *Geomech. Eng.*, **7**(4), 375-401. https://doi.org/10.12989/gae.2014.7.4.375.
Zhang, Q., Li, Y.J., Yu, M. W., Hu, H.H. and Hu, J.H. (2015), "Study of the rock foundation stability of the Aizhai suspension bridge over a deep canyon area in China", *Eng. Geol.*, **198** 65-77. https://doi.org/10.1016/j.enggeo.2015.09.012.

GC